Geomechanics and Engineering, *Vol. 24, No. 1 (2021) 57-65*
DOI: https://doi.org/10.12989/gae.2021.24.1.057

DEM study on effects of fabric and aspect ratio on small strain stiffness of granular soils

Jian Gong*[1,2], Liang Li[2], Lianheng Zhao[2], Jinfeng Zou[2] and Zhihong Nie[2]

[1]*College of Civil Engineering and Architecture, Guangxi University, Guangxi, China*
[2]*School of Civil Engineering, Central South University, Hunan, China*

(Received September 11, 2019, Revised December 22, 2020, Accepted December 24, 2020)

Abstract. The effects of initial soil fabric and aspect ratio (AR) on the small-strain stiffness (G_0) of granular soils are studied by employing discrete element method (DEM) numerical analysis. Elongated clumps composed of subspheres were adopted, and the G_0 values were obtained by DEM simulations of drained triaxial tests under different densities and initial confining pressure (p_0). The DEM simulations indicate that the initial soil fabric has an insignificant effect on G_0. The effect of the AR on G_0 is related to the initial density. Namely, for dense specimens, G_0 first increases with increasing AR, reaching a plateau value when the AR ≥ 1.5. However, for loose specimens, G_0 gradually increases as the AR increases. Microscopic examination reveals that G_0 uniquely depends on the coordination number of the particles (CN-particle) rather than the subspheres (CN-sphere) at the particulate level for the effects of initial soil fabric and AR. Finally, Poisson's ratio ν_0 is also determined by CN-particle. In addition, based on data in literature and this study, ν_0 can be fitted as $\nu_0 = 5.920(G_0/(p_0)^{1/3})^{-0.99}$, which can be used to predict ν_0 of granular soils based on the measured G_0.

Keywords: inherent anisotropy; aspect ratio; small-strain stiffness; Poisson's ratio; granular soils; DEM

1. Introduction

Small-strain stiffness (G_0) is a basic soil property that is important in a variety of geotechnical applications, such as earthquake site response analyses and liquefaction potential evaluations. Many studies (e.g., Chuang *et al.* 1984, Hardin and Richart 1963, Iwasaki and Tatsuoka 1977, Lo Prresti *et al.* 1997) have been conducted to investigate the effects of various factors on G_0 of soils through well-controlled experiments on sand. It is well recognized that the void ratio e and the mean effective stress p_0 are the most important factors influencing G_0. Recently, there has been growing interest in understanding the effects of particle characteristics on G_0, such as the effects of particle size (e.g., Patel and Bartake 2008, Wichtmann and Triantafyllidis 2009, Yang and Gu 2013), gradation (e.g., Wichtmann and Triantafyllidis 2009), particle shape (e.g., Cho *et al.* 2006, Liu and Yang 2018) and fines content (e.g., Gong *et al.* 2019a, Goudarzy *et al.* 2016, Yang *et al.* 2018).

Inherent anisotropy (i.e., initial soil fabric), refers to the initial spatial arrangement of particles, is a common phenomenon in granular soils. This phenomenon is generally initiated by the deposition of particles under gravity, and the long axis of soils tends to align in a specific direction (Mitchell and Soga 2005). Prior experimental (e.g., Flitti *et al.* 2019, Guo 2008, Tong *et al.* 2014) and numerical studies (e.g., Fu and Dafalias 2011, Yang *et al.* 2013) have produced valuable data showing the effect of inherent anisotropy on the mechanical behaviours of granular soils. However, investigations on the effect of inherent anisotropy on G_0 of granular soils are relatively rare. Furthermore, it appears that there is no consensus regarding the effect of inherent anisotropy on G_0. For example, through a group of laboratory tests, Yamashita *et al.* (2005) and Li and Zeng (2014) stated that the G_0 value for a specimen prepared at 90° is larger than that for a 0° deposition angle. However, Yu *et al.* (2013) and Li *et al.* (2014) reported that granular materials with larger deposition angles had higher liquefaction potential, suggesting that granular materials with larger deposition angles may have smaller G_0 values. These diverse conclusions may be attributed to the fact that it is difficult to isolate the inherent anisotropy effect in the laboratory tests. For example, Yamashita *et al.* (2005) prepared two types of sand with different shapes and particle size distributions at 90° and 0° deposition angles. As a result, it was found that the responses of G_0 with respect to the deposition angle were different for these two sands. In this context, whether the G_0 values of granular soils are dependent on inherent anisotropy remains unclear and needs to further study.

The discrete element method (DEM for short) proposed by Cundall and Strack (1979) offers an alternative way to isolate the inherent anisotropy effect and provides microscopic information that is not easily available from laboratory tests. The DEM has previously been demonstrated to reproduce certain key features of granular soils and reveal many macroscopic soil behaviours at the particulate level, such as the shear behaviours of granular soils (Kumara and Hayano 2016, Gong and Liu 2017, Gong

*Corresponding author, Ph.D.
E-mail: gj_csu@hotmail.com

ISSN: 2005-307X (Print), 2092-6219 (Online)

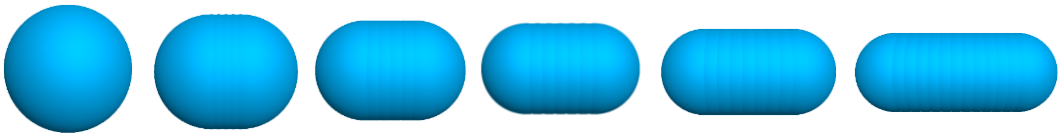

Fig. 1 Elongated particles used in the DEM simulations. From left to right, particles have ARs of 1.00, 1.25, 1.50, 1.75, 2.00 and 2.50, and the number of subspheres used to create these various ARs are 1, 5, 6, 7, 9 and 13, respectively

Table 1 Input parameters in the DEM simulations

Parameter	Value
Particle density, ρ	2500 kg/m^3
No. of particles	4000
Shear modulus, G	29 GPa
Poisson's ratio, ν	0.15
Friction coefficient between clumps	0.5
Friction coefficient between clump-wall	0.0
Damping constant	0.7

et al. 2019b, Rahman *et al.* 2018, Qu *et al.* 2019, Qian *et al.* 2020) and small-strain properties of sands (Gong *et al.* 2019a, Gu and Yang 2018, Nguyen *et al.* 2018). Alternatively, it is well known that inherent anisotropy is related to the aspect ratio (AR) of soils (ratio of major to minor axis), i.e., soils with a high AR tend to lie flat to minimize their gravitational potential energy. Thus, it is an interesting issue whether the AR will influence G_0 of granular soils at a given inherent anisotropy. Gu *et al.* (2017) noted that G_0 depends uniquely on a soil's mechanical coordination number (CN, i.e., the average number of contacts per particle). Previous experimental (e.g., Donev *et al.* 2004, Donev *et al.* 2007) and numerical studies (e.g., Gong and Liu 2017) indicated that for true and multisphere ellipsoids, the CN first increases with the AR, reaching a plateau value when the AR ≥ 1.5. These findings suggest that the G_0 value may first increase with AR and remain constant when the AR ≥ 1.5. However, Liu and Yang (2018) found that the G_0 values of sands generally increase with increasing AR, which is inconsistent with the predicted tendency. The difference may be attributed to the fact that the ARs of the tested sands in Liu and Yang (2018) were in a narrow range (i.e., from 1.31 to 1.34). In fact, the ARs of natural granular soils may be distributed in a wide range. For example, Altuhafi *et al.* (2016) measured a database of 25 natural sands and found that the ARs of these sands range from 1.07 to 1.50. Furthermore, Stahl and Konietzky (2011) tested two types of gravels and reported that the ARs of these gravels range from 1.0 to 2.5. To obtain the effect of the AR on G_0 of granular soils, a wide range of AR should be considered. These needs are the motivation of this work, wherein we conduct grain-scale modelling using the DEM. Taking advantage of DEM simulations, the microstructure information of granular soils can be conveniently obtained. On this basis, the DEM can capture how the inherent anisotropy and AR of granular soils affect the microstructure and thus influence G_0, which constitutes the main aim of this investigation.

In this study, the effects of inherent anisotropy and AR of soils on G_0 of granular soils are investigated by conducting DEM analysis of an assembly of multisphere elongated clumps. DEM specimens with different initial inherent anisotropy and particle ARs were prepared at two different densities (dense and loose), and quasi-static drained triaxial compression tests were simulated. The discussion focuses on studying the underlying mechanisms of the effects of inherent anisotropy and AR of particles on G_0 of granular soils. Finally, the empirical relationship between Poisson's ratio ν_0 and G_0 is explored, this relationship can be used to predict ν_0 of granular soils based on the measured G_0.

2. DEM modelling

The well-recognized DEM program PFC^{3D} (Itasca 2014) was used to perform the numerical simulations. Elongated particles with different ARs were simulated by multisphere clumps, as displayed in Fig. 1. The nonlinear Hertz-Mindlin contact law was used to capture the stress-dependent G_0. The shear modulus and Poisson's ratio of the subspheres were set to 29 GPa and 0.15, respectively, which were also used in previous DEM simulations to investigate the small-strain properties of granular soils (i.e., Gong *et al.* 2019a, Gu and Yang 2018). To eliminate the potential effect of particle size distribution on G_0 of granular soils, a monodisperse distribution of particles was used. All elongated particles had the same volume, equal to the volume of a sphere with diameter D = 2 mm. All basic parameters used in this study are listed in Table 1.

The specimens were modelled by the isotropic compression method. To prepare specimens with different deposition angles (0°, 15°, 30°, 45°, 60°, 75° and 90°), particles with an AR = 1.50 and orientation at a given deposition angle were initially generated within a cube, with zero contacts and no gravity, as shown in Figs. 2(a) and 2(b). The cube was modelled using six rigid walls. Each specimen was limited to 4000 particles considering the computational cost. This number of particles was consistent with the similar numbers of spheres used in Gong *et al.*

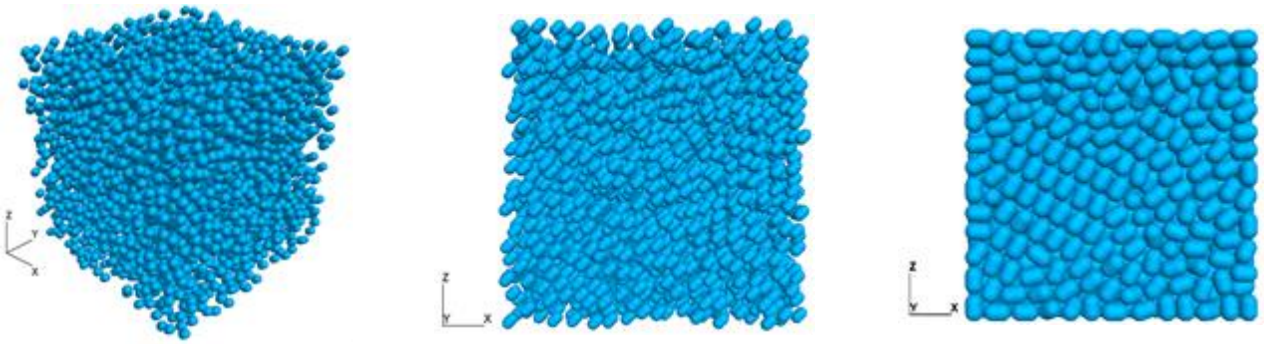

(a) (b) (c)

Fig. 2 Dense specimen generation at 45° deposition angle: (a) initial stage at isometric view, (b) initial stage at view of negative y-direction and (c) finial stage

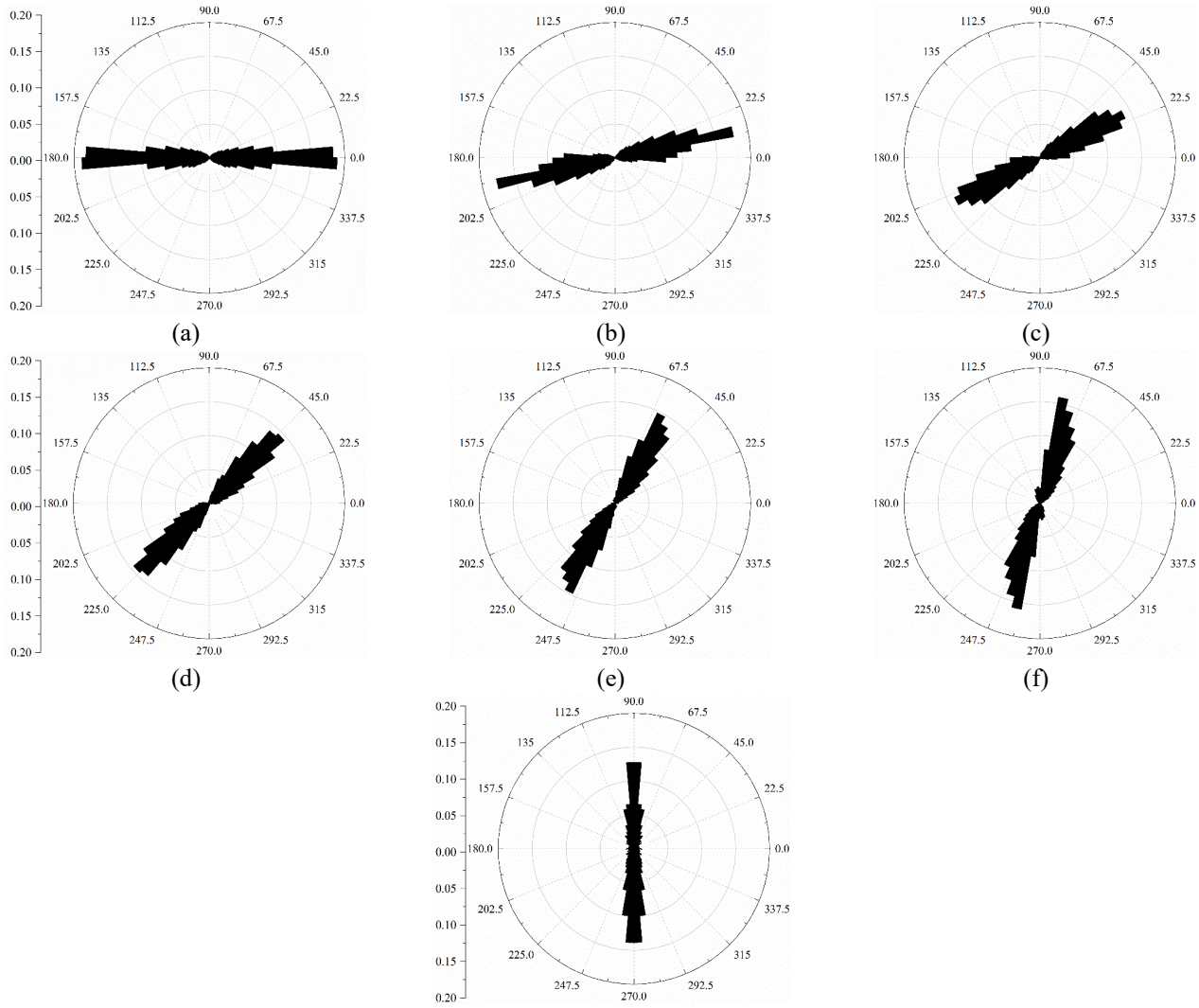

(a) (b) (c)

(d) (e) (f)

(g)

Fig. 3 The probability density of particle orientation of initial dense specimens associated with different deposition angles: (a) 0°, (b) 15°, (c) 30°, (d) 45°, (e) 60°, (f) 75° and (g) 90°

(2019a). All particles were subjected to isotropic compression with a low strain rate through a servo control mechanism that acted on the walls. During the initial isotropic compression, the particle rotation was inhibited while the ratio of the mean static unbalanced force to the mean contact force was less than 10^{-3}. Then, the restriction of particle rotation was removed. The specimens were compressed to the desired confining pressure p_0 and were considered to be equilibrated when the ratio of the mean static unbalanced force to the mean contact force was less

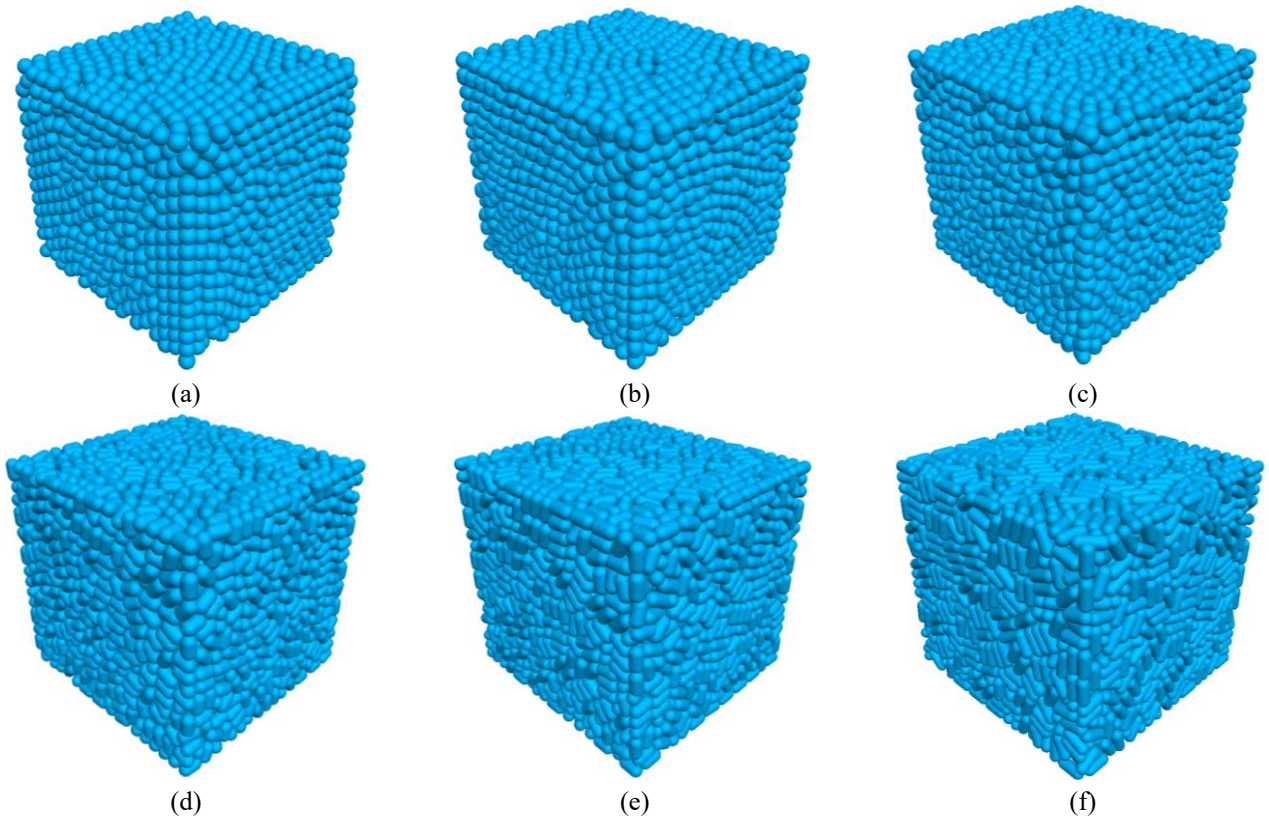

Fig. 4 The configurations for various ARs: (a) AR=1.0, (b) AR=1.25, (c) AR=1.50, (d) AR=1.75, (e) AR=2.00 and (f) AR=2.5

than 10^{-5}. In DEM simulations, low inter-particle friction coefficient generates dense sample, while high inter-particle friction coefficient generates loose sample. In this study, the friction coefficients between particles were set to 0.0 and 0.5 to obtain isotropically dense and loose specimens, respectively. After equilibration (as shown in Fig. 2(c)), the specimen were considered to be in the initial specimen state. Fig. 3 illustrates the probability density of the particle orientation of initial dense specimens associated with different deposition angles. The angle indicates the angle between the particle orientation and the positive x-direction. For each deposition angle, the initial preferred particle orientations generally coincide with the deposition angle. Furthermore, it can be observed that the initial fabric intensities of the specimens are almost the same. The particle orientations of loose particles exhibit the same trend but are not shown here. Alternatively, to prepare specimens with different ARs, particles with random orientations were initially generated within a cube, with zero contacts and no gravity. Then, the isotropic compression method was conducted until the specimens reached equilibration. The respective specimen configurations for various ARs are exhibited in Fig. 4. Note that the initial fabric intensities of specimens with different deposition angle and ARs are the same, which excluded the effect of fabric intensities caused by the particle relocation during formation of fabric soils. This effect will be investigated in further study.

Following a procedure equivalent to that used in laboratory experiments Hoque and Tatsuoka (1998), the initial specimens were subjected to a drained triaxial test. During the loading, a very small strain increment $\Delta\varepsilon_1$ was applied, while the lateral stresses were kept constant by servo control until the shear strain ($\gamma = \Delta\varepsilon_1\text{-}0.5(\Delta\varepsilon_2+\Delta\varepsilon_3)$) reached 10^{-6}, where $\Delta\varepsilon_2$ and $\Delta\varepsilon_3$ represent the strain increments of the two lateral directions, respectively. Then, G_0 and Poisson's ratio ν_0 can be calculated as follows:

$$G_0 = \frac{\Delta\sigma_1/2}{\gamma} \tag{1}$$

$$\upsilon_0 = \frac{\Delta\varepsilon_3}{\Delta\varepsilon_1} \tag{2}$$

where $\Delta\sigma_1$ represents the axial stress increment and $\Delta\varepsilon_1$ and $\Delta\varepsilon_3$ represent the axial and lateral strain increments, respectively.

3. Results and discussion

In this study, the small-stiffness properties of granular soils are studied by DEM simulations using elongated particles, which are different from the spherical particles used in previous DEM simulations (e.g., Gong *et al.* 2019a). Therefore, primarily, it is necessary to validate whether multisphere elongated particles can capture the stress-dependent and void ratio-dependent G_0. Fig. 5 shows G_0 of specimens with an AR=1.5 at different confining pressures and initial void ratios. For comparison, data extracted from Gu *et al.* (2017) for spheres are also included. As expected, in Gu *et al.* (2017) and this study, G_0 increases with increasing p_0 and decreasing void ratio on a log-log scale. This finding indicates that our simulations using elongated

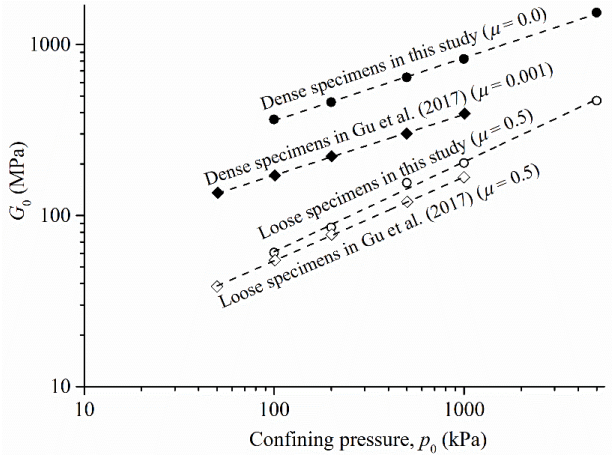

Fig. 5 The small-strain stiffness G_0 of dense and loose specimens with AR=1.5

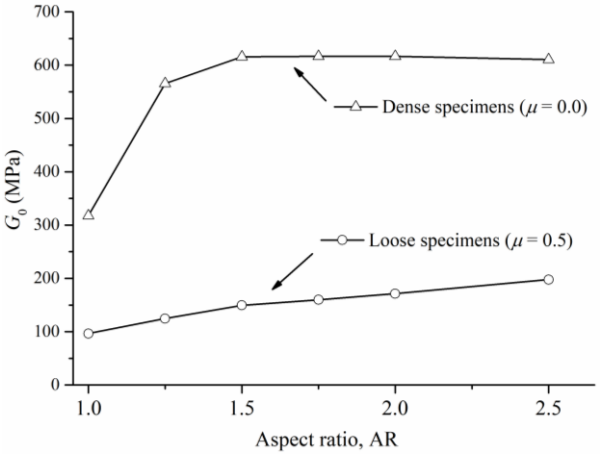

Fig. 8 Relationship between G_0 and AR for dense and loose specimens

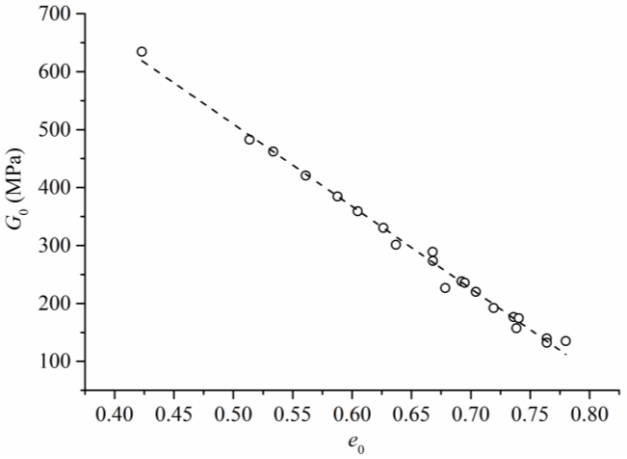

Fig. 6 Graph showing the relationship between G_0 and e_0 at AR = 1.5 and p_0 = 500 kPa

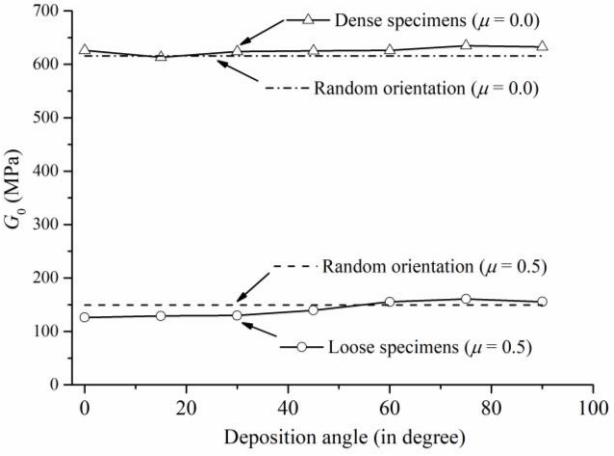

Fig. 7 The G_0 for dense and loose specimens versus the deposition angle at p_0 = 500 kPa

can successfully capture the stress-dependent G_0. In addition, G_0 can be expressed by a power law of p_0 for dense and loose specimens (i.e., $G_0=A_0(p_0)^n$, where A_0 and n are two fitting parameters), which is consistent with previous experimental results (e.g., Chuang *et al.* 1984, Hardin and Richart 1963). Alternatively, at a given p_0, the G_0 values for an AR=1.5 in this study are always greater than those in Gu *et al.* (2017) for spheres, and this result is more obvious for dense specimens. This finding is attributed to the particle shape effect, which is discussed in a later section. Fig. 6 illustrates the relationship between G_0 and the initial void ratio (e_0) at an AR = 1.5 and p_0 = 500 kPa. Different e_0 values are generated using different μ (ranges from 0.0 to 0.525) during isotropic compression in this study. The G_0 values linearly decrease with respect to e_0, this finding is consistent with previous experimental (i.e., Goudarzy *et al.* 2016, Yang and Liu 2016) and numerical results (i.e., Gong *et al.* 2019a), indicating that elongated particles can also successfully capture the void ratio-dependent G_0.

Fig. 7 illustrates G_0 of dense and loose specimens versus the deposition angle at p_0 = 500 kPa. The G_0 values of random orientation specimens are also included. It is clear that G_0 remains nearly unchanged for various deposition angles, despite slight fluctuations. In addition, for both dense and loose specimens, the G_0 values of random orientation specimens approach the G_0 values of specimens at a given deposition angle. These findings indicate that the G_0 values of granular soils are independent of inherent anisotropy, which is different from the observations in Yamashita *et al.* (2005) and Li and Zeng (2014) that the G_0 value of a specimen prepared at 90° is larger than that of a 0° deposition angle. These different conclusions may be related to noise factors, such as the particle distribution size effect in Yamashita *et al.* (2005) and Li and Zeng (2014). Indeed, Wichtmann and Triantafyllidis (2009) and Gu *et al.* (2017) reported that at the same confining pressure and void ratio, the G_0 value decreases as the coefficient of uniformity of the soil increases. Fig. 8 plots the relationship between G_0 and the AR for dense and loose specimens. It can be observed that G_0 exhibits different trends for dense and loose specimens. Specifically, for dense specimens, G_0 first increases with increasing AR, reaching a plateau value when the AR ≥ 1.5. However, for loose specimens, G_0 gradually increases as the AR increases. On the other hand, when the AR increases from 1.0 to 2.5, G_0 increases from 96 MPa to 198 MPa for loose specimens and 320 MPa to

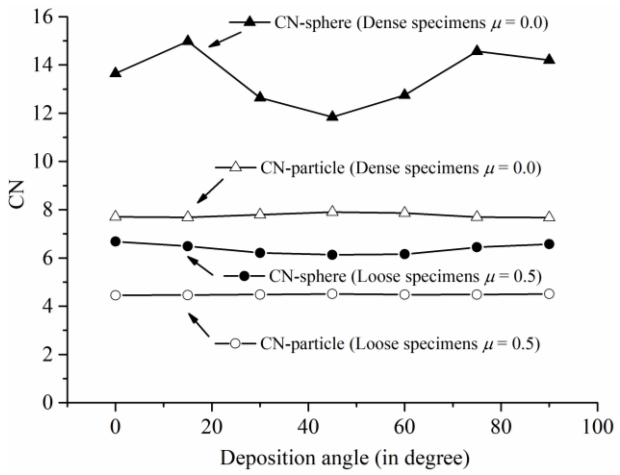

(a)

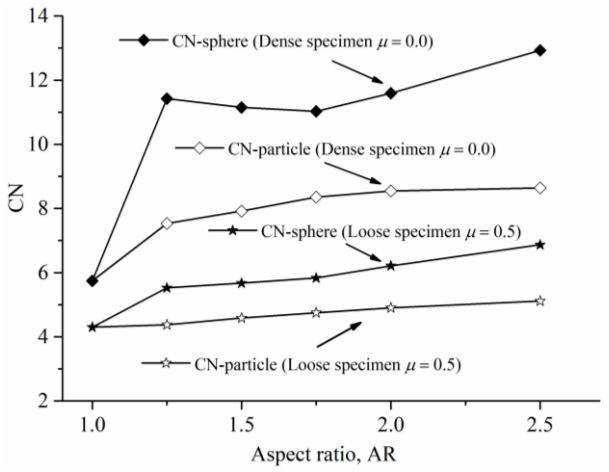

(b)

Fig. 9 Relationship between (a) CN and deposition angle and (b) CN and AR

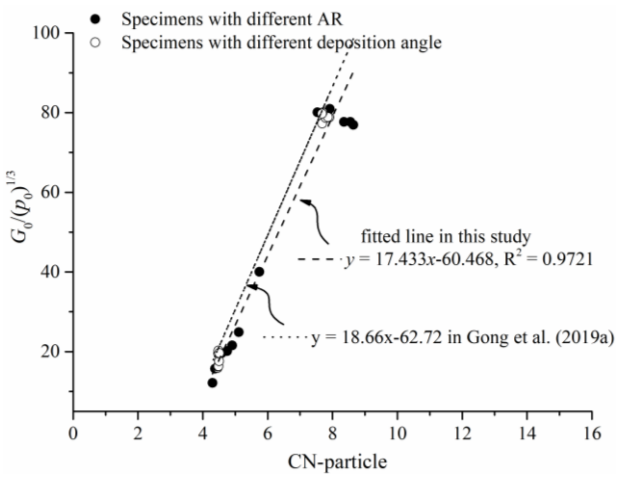

(a)

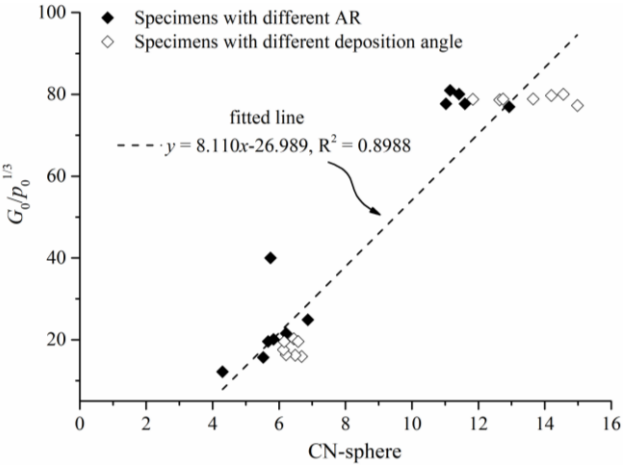

(b)

Fig. 10 Relationship between the stress-normalized shear modulus $G_0/(p_0)^{1/3}$ versus (a) CN-particle and (b) CN-sphere

610 MPa for dense specimens, indicating that the increase in G_0 with the AR is more significant in dense specimens.

Conceptually, the stiffness of granular soils depends on the stiffness of a single contact and the number of contacts. In this study, using the Hertz-Mindlin contact model, the stiffness of a single contact is determined by the particle properties, which are the same for particles with different deposition angles and ARs. Therefore, it is expected that the soil stiffness is related to the number of contacts. Gu *et al.* (2017) reported that the G_0 values of granular soils uniquely depend on their mechanical CN (i.e., the average number of contacts per particle). Indeed, when using a multisphere approach to model nonspherical particles, there are two different approaches to calculate the CNs. The first approach is the conventional "particle-particle" approach (marked as CN-particle), which defines the CN as the number of contacts between different composite particles (not between the constituent subspheres) divided by the number of particles. The other approach is the "sphere-sphere" approach (marked as CN-sphere), which defines the CN as the total number of contacts between the subspheres divided by the number of particles.

Figs. 9(a) and 9(b) illustrate the relationships between CN and deposition angle and CN and AR, respectively. Referring to the inherent anisotropy effect, Fig. 9(a) shows that CN-particle is nearly unchanged with the deposition angle for both dense and loose specimens. In addition, CN-sphere remains constant for loose specimens but shows great fluctuation for dense specimens. The unchanged CN-particle is similar to that shown by the relationship between G_0 and deposition angle, as shown in Fig. 7. Referring to the particle shape effect, Fig. 9(b) shows that CN-sphere and CN-particle exhibit slightly different trends with the AR for both dense and loose specimens. That is, when the AR ≥ 1.75, CN-particle remains unchanged, but CN-sphere increases for dense specimens; both CN-particle and CN-sphere gradually increase for loose specimens, but the increase is more obvious for CN-sphere, which is attributed to the fact that longer particles contain many more subspheres. G_0 and CN-particle with the AR show generally similar trends for dense and loose specimens, as shown in Fig. 8 and Fig. 9(b). Therefore, it is believed that the change in G_0 can be explained by the change in CN-particle. Based on a series of DEM simulations, Gong *et al.* (2019) and Magnanimo *et al.* (2008) reported that G_0 of granular materials is a function of the CN.

For a better illustration of the underlying mechanisms of

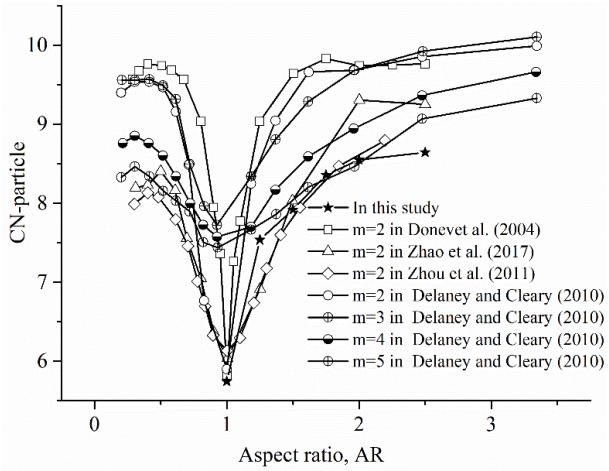

Fig. 11 The relationship between CN-particle and AR in this study and literatures

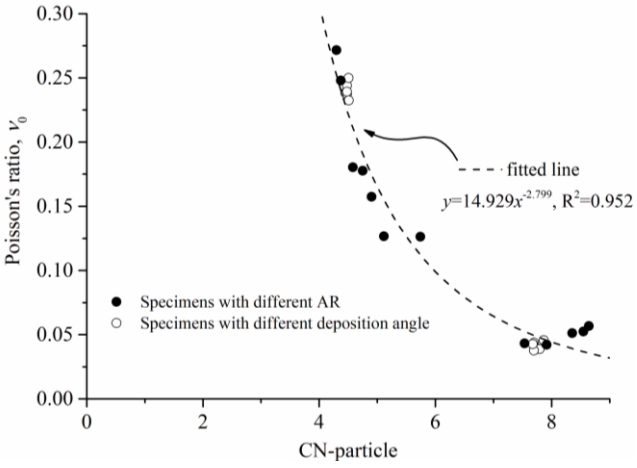

Fig. 12 Relationship between ν_0 and the CN-particle

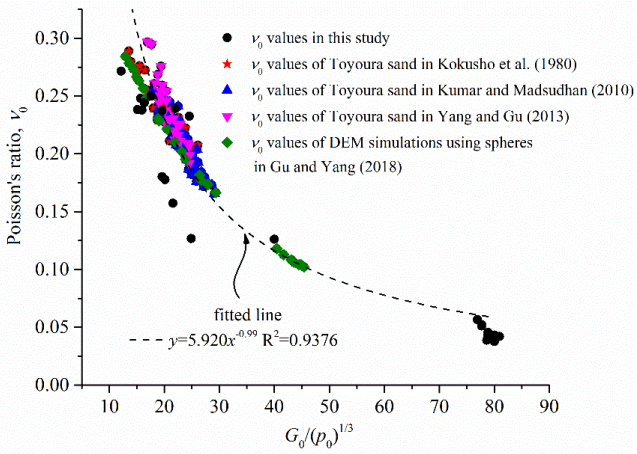

Fig. 13 Relationship between ν_0 and $G_0/(p_0)^{1/3}$ in this study and literature

the change in G_0, the stress-normalized shear modulus $G_0/(p_0)^{1/3}$ is plotted versus CN-particle and CN-sphere in Figs. 10(a) and 10(b), respectively. For comparison, the published data in Gong *et al.* (2019) for gap-graded soils using spheres are included in Fig. 10(a). It is clear that $G_0/(p_0)^{1/3}$ can be fitted by linear functions of CN-particle and CN-sphere, expressed as $y = 17.433x$-60.468 and $y = 8.110x$-26.989, respectively. In addition, the R^2 value of the fitted line for CN-particle (= 0.9721) is greater than that for CN-sphere (=0.8988), indicating that CN-particle provides a better linear relationship with $G_0/(p_0)^{1/3}$ than CN-sphere. The linear relationship convincingly suggests that the effects of inherent anisotropy and particle shape on G_0 of granular soils are mainly related to CN-particle at the particle level. Furthermore, the fitted line for CN-particle in this study is close to that in Gong *et al.* (2019), indicating that the dependence of G_0 on CN-particle is also applicable to gap-graded granular soils. Superellipsoids are defined as $(x/a)^m+(y/b)^m+(z/c)^m=1$, where a, b and c are the semi-major axis lengths and m is the shape parameter. In this study, only prolate ellipsoids (i.e., $a > b = c$, m = 2) are considered. Fig. 11 displays the CN-particle values of oblate and prolate superellipsoids extracted from literature (i.e., Donev, *et al.* 2004, Zhao *et al.* 2017, Zhou *et al.* 2011, Delaney and Cleary 2010), with the aim to systematically predict the variation trend of G_0 with respect to the AR. As the AR increases from 1.0 for m = 2 in the literature and this study, CN-particle increases to a peak and then remains at a steady value for further increases in the AR. However, for m = 3, 4 and 5, CN-particle gradually increases with increasing AR. Alternatively, as the AR decreases from 1.0 for all cases of m in the literature and this study, CN-particle increases to a peak and then slowly decreases. Based on the linear relationship between G_0 and CN-particle mentioned above, it is reasonable to infer that G_0 will exhibit the same trend as the AR, as shown in Fig. 11.

Fig. 12 presents the variation in Poisson's ratio ν_0 with CN-particle for dense and loose granular soils in this study. Note that Fig. 12 includes different ARs (i.e., 1.00, 1.25, 1.50, 1.75, 2.00 and 2.50) and deposition angles (i.e., 0°, 15°, 30°, 45°, 60°, 75° and 90°). It is clear that ν_0 gradually decreases with CN-particle. In addition, there is a unique power function fitting ν_0 and CN-particle for all specimens, i.e., $y = 14.929x^{-2.799}$. This finding indicates that ν_0 also depends on CN-particle. Considering that both G_0 and ν_0 are determined by CN-particle, the ν_0 values of the specimens are plotted versus $G_0/(p_0)^{1/3}$ in Fig. 13. Note that Fig. 13 also includes different ARs (i.e., 1.00, 1.25, 1.50, 1.75, 2.00 and 2.50) and deposition angles (i.e., 0°, 15°, 30°, 45°, 60°, 75° and 90°). For comparison, the measured data of Toyoura sands (i.e., Kokusho *et al.* 1980, Kumar and Madhusudhan 2010, Yang and Gu 2013) and DEM simulations using spheres (i.e., Gu and Yang 2018) are also superimposed. The relationship between ν_0 and $G_0/(p_0)^{1/3}$ is nearly the same in this study and literature. As $G_0/(p_0)^{1/3}$ increases, ν_0 exponentially decreases. The fitted line of the measured data in the laboratory tests and DEM simulations is $y = 5.920x^{-0.99}$. In practice, this relationship can be used to predict ν_0 of granular soils based on the measured G_0.

4. Conclusions

In this study, the effects of initial soil fabric and AR on the small-strain stiffness (G_0) of granular soils were investigated by DEM simulations. Elongated clumps

composed of subspheres were adopted, and the G_0 values were obtained by numerical drained triaxial tests. The main findings of this study are summarized below:

(1) The verification tests show that G_0 increases with increasing p_0 and linearly decreasing void ratio on a log-log scale, and this result is consistent with previous experimental and numerical studies. This finding indicates that a clump composed of subspheres can successfully capture the stress-dependent and void ratio-dependent G_0.

(2) The DEM simulations indicate that the initial soil fabric has an insignificant effect on G_0. In addition, the effect of the AR on G_0 is related to the initial density. Specifically, G_0 first increases with increasing AR, reaching a plateau value when the AR ≥ 1.5 for dense specimens. However, G_0 continuously increases as the AR increases for loose specimens. Microscopic analysis reveals that G_0 uniquely depends on the coordination number of the particles (CN-particle) rather than the subspheres (CN-sphere) at the particulate level.

(3) The DEM simulations show that Poisson's ratio ν_0 is also determined by CN-particle. In addition, based on data in the literature and this study, it is found that ν_0 can be fitted as $\nu_0 = 5.920(G_0/(p_0)^{1/3})^{-0.99}$. This expression is useful and can be applied to predict ν_0 of granular soils based on the measured G_0.

Acknowledgments

This research is supported by the National Natural Science Foundation of China (No. 51809292, 51478481 and 51878668), Postdoctoral Fund of Central South University (No. 205455) and Beijing Municipal Science and Technology Project: Research and Application of Design and Construction Technology of Railway Engineering Traveling the Rift Valley (No. Z181100003918005). The authors would like to express their appreciation to the financial assistance.

References

Altuhafi, F.N., Coop, M.R. and Georgiannou, V.N. (2016), "Effect of particle shape on the mechanical behavior of natural sands", *J. Geotech. Geoenviron. Eng.*, **142**(12), 04016071. http://doi.org/10.1061/(ASCE)GT.1943-5606.0001569.

Cho, G.C., Dodds, J. and Santamarina, J.C. (2006), "Particle shape effects on packing density, stiffness, and strength: Natural and crushed sands", *J. Geotech. Geoenviron. Eng.*, **132**(5), 591-602. http://doi.org/ 10.1061/(ASCE)1090-0241(2006)132:5(591).

Chuang, R.M., Yokel, F.Y. and Drnevich, V.P. (1984), "Evaluation of dynamic properties of sands by resonant column testing", *Geotech Test J*, **2**(7), 60-69. http://doi.org/10.1520/GTJ10594J.

Cundall, P.A. and Strack, O.D.L. (1979), "A discrete numerical model for granular assemblies", *Géotechnique*, **29**(1), 47-65. http://doi.org/10.1680/geot.1980.30.3.331.

Delaney, G.W. and Cleary, P.W. (2010), "The packing properties of superellipsoids", *Europhys. Lett.*, **89**(3), 340023. https://doi.org/10.1209/0295-5075/89/34002.

Donev, A., Cisse, I., Sachs, D., Variano, E., Stillinger, F.H., Connelly, R., Torquato, S. and Chaikin, P.M. (2004), "Improving the density of jammed disordered packings using ellipsoids", *Science*, **303**(5660), 990-993. http://doi.org/10.1126/science.1093010.

Donev, A., Connelly, R., Stillinger, F.H. and Torquato, S. (2007), "Underconstrained jammed packings of nonspherical hard particles: Ellipses and ellipsoids", *Phys. Rev. E*, **75**(5), 05130451. http://doi.org/ 10.1103/PhysRevE.75.051304.

Flitti, A., Della, N., De Kock, T., Cnudde, V. and Verastegui-Flores, R.D. (2019), "Effect of initial fabric on the undrained response of clean Chlef sand", *Eur. J. Environ. Civ. Eng.*, 1-16. http://doi.org/10.1080/19648189.2019.1631217.

Fu, P. and Dafalias, Y.F. (2011), "Study of anisotropic shear strength of granular materials using DEM simulation", *Int. J. Numer. Anal. Meth*, **35**(10), 1098-1126. http://doi.org/10.1002/nag.945.

Gong, J, and Liu, J. (2017), "Mechanical transitional behavior of binary mixtures via DEM: Effect of differences in contact-type friction coefficients", *Comput. Geotech.*, **85**, 1-14. http://doi.org/ 10.1016/j.compgeo.2016.12.009.

Gong, J. and Liu, J. (2017), "Effect of aspect ratio on triaxial compression of multi-sphere ellipsoid assemblies simulated using a discrete element method", *Particuology*, **32**, 49-62. http://doi.org/ 10.1016/j.partic.2016.07.007.

Gong, J., Jun, L. and Liang, C. (2019b), "Shear behaviors of granular mixtures of gravel-shaped coarse and spherical fine particles investigated via discrete element method", *Powder Technol.*, **353**, 178-194. http://doi.org/10.1016/j.powtec.2019.05.016.

Gong, J., Wang, X., Li, L. and Nie, Z. (2019a), "DEM study of the effect of fines content on the small-strain stiffness of gap-graded soils", *Comput. Geotech.*, **112**, 35-40. http://doi.org/ 10.1016/j.compgco.2019.04.008.

Goudarzy, M., Koenig, D. and Schanz, T. (2016), "Small strain stiffness of granular materials containing fines", *Soils Found.*, **56**(5), 756-764. http://doi.org/10.1016/j.sandf.2016.08.002.

Gu, X.Q. and Yang, S. (2018), "Why the OCR may reduce the small strain shear stiffness of granular materials?", *Acta Geotech.*, **13**(6), 1467-1472. http://doi.org/10.1007/s11440-018-0695-9.

Gu, X.Q., Lu, L. and Qian, J. (2017), "Discrete element modeling of the effect of particle size distribution on the small strain stiffness of granular soils", *Particuology*, **32**, 21-29. http://doi.org/ 10.1016/j.partic.2016.08.002.

Guo, P. (2008), "Modified direct shear test for anisotropic strength of sand", *J. Geotech. Geoenviron. Eng.*, **134**(9), 1311-1318. http://doi.org/10.1061/(ASCE)1090-0241(2008)134:9(1311).

Hardin, B.O. and Richart, F.E. (1963), "Elastic wave velocities in granular soils", *J. Soil Mech. Found. Div.*, **89**(SM1), 39-56.

Hoque, E. and Tatsuoka, F. (1998), "Anisotropy in elastic deformation of granular materials", *Soils Found.*, **38**(1), 163-179. http://doi.org/10.3208/sandf.38.163.

Itasca. (2014), *User's manual for PFC3D*, Itasca Consulting Group, Inc., Minneapolis, Minnesota, U.S.A.

Iwasaki, T. and Tatsuoka, F. (1977), "Effects of grain size and grading on dynamic shear moduli of sands", *Soils Found.*, **3**(17), 19-35. http://doi.org/10.3208/sandf1972.17.3_19.

Jiang, M. Zhang, A. and Fu, C. (2018), "3D DEM simulations of drained triaxial tests on inherently anisotropic granulates", *Eur. J. Environ. Civ. Eng.*, **221**(SI), s37-s56. http://doi.org/10.1080/19648189.2017.1385541.

Kokusho, T. (1980), "Cyclic triaxial test of dynamic soil properties for wide strain range", *Soils Found.*, **2**(20), 45-60. http://doi.org/10.1016/0148-9062(81)91053-6.

Kumar, J. and Madhusudhan, B.N. (2010), "Effect of relative density and confining pressure on Poisson ratio from bender and extender elements tests", *Geotechnique*, **60**(7), 561-567. http://doi.org/ 10.1680/geot.9.T.003.

Kumara, J.J. and Hayano, K. (2016), "Importance of particle shape

on stress-strain behaviour of crushed stone-sand mixture", *Geomech. Eng.*, **10**(4), 455-470. http://doi.org/10.12989/gae.2016.10.4.455.

Li, B. and Zeng, X. (2014), "Effects of fabric anisotropy on elastic shear modulus of granular soils", *Earthq. Eng. Eng. Vib.*, **13**(2), 269-278. http://doi.org/10.1007/s11803-014-0229-x.

Li, B., Zeng, X. and Yu, H. (2014), "Characterization of liquefaction resistance of sand: Effect of initial fabric", *J. Earthq. Tsunami*, **8**(1), 14500011. http://doi.org/10.1142/S1793431114500018.

Liu, X. and Yang, J. (2018). "Shear wave velocity in sand: Effect of grain shape", *Geotechnique*, **68**(8), 742-748. http://doi.org/10.1680/jgeot.17.T.011.

Lo Prresti, D.C.F., Jamiolkowski, M., Parrara, O. and Predroni, A.C.S. (1997), "Shear modulus and damping of soils", *Geotechnique*, **3**(47), 603-617. http://doi.org/10.1680/geot.1997.47.3.603.

Magnanimo, V., La Ragione, L., Jenkins, J.T., Wang, P. and Makse, H.A. (2008), "Characterizing the shear and bulk moduli of an idealized granular material", *Europhys. Lett.*, **81**(3), 340063. http://doi.org/10.1209/0295-5075/81/34006.

Mitchell, J. and Soga, K. (2005), *Fundamentals of Soil Behavior*, John Wiley & Sons, New York, U.S.A.

Nguyen, C., O'Sullivan, C. and Otsubo, M. (2018), "Discrete element method analysis of small-strain stiffness under anisotropic stress states", *Geotechnique Lett.*, **8**(3), 183-189. https://doi.org/10.1680/jgele.17.00122.

Patel, A., Bartake, P.P. and Singh, D.N. (2008), "An empirical relationship for determining shear wave velocity in granular materials accounting for grain morphology", *Geotech. Test. J.*, **32**(1), 1-10. http://doi.org/ 10.1520/GTJ100796.

Qian, J., Yao, Y., Li, J., Xiao, H.B. and Luo, S.P. (2020), ''Resilient properties of soil-rock mixtures materials: Preliminary investigation of the effect of composition and structure'', *Materials*, **13**(7), 1658, http://doi.org/10.3390/ma13071658.

Qu, T.M., Feng, Y.T., Wang, Y. and Wang, M. (2019), "Discrete element modelling of flexible membrane boundaries for triaxial tests", *Comput. Geotech.*, **115**, 103154. http://doi.org/10.1016/j.compgeo.2019.103154.

Rahman, M.M., Nguyen, H.B.K. and Rabbi, A.T.M.Z. (2018), "The effect of consolidation on undrained behaviour of granular materials: Experiment and DEM simulation", *Geotech. Res.*, **5**(4), 199-217. http://doi.org/10.1680/jgere.17.00019.

Stahl, M. and Konietzky, H. (2011), "Discrete element simulation of ballast and gravel under special consideration of grain-shape, grain-size and relative density", *Granul. Matter*, **13**(4), 417-428. http://doi.org/10.1007/s10035-010-0239-y.

Tong, Z., Fu, P., Zhou, S. and Dafalias, Y.F. (2014), "Experimental investigation of shear strength of sands with inherent fabric anisotropy", *Acta Geotech.*, **9**(2), 257-275. http://doi.org/10.1007/s11440-014-0303-6.

Wichtmann, T. and Triantafyllidis, T. (2009), "Influence of the grain-size distribution curve of quartz sand on the small strain shear modulus G_{max}", *J. Geotech. Geoenviron. Eng.*, **135**(10), 1404-1418. http://doi.org/10.1061/(ASCE)GT.1943-5606.0000096.

Yamashita, S., Hori, T. and Suzuki, T. (2005), "Effects of initial and induced anisotropy on initial stiffness of sand by triaxial and bender elements tests", *Proceedings of the 1st Japan-U.S. Workshop on Testing, Modeling, and Simulation*, Boston, Massachusetts, U.S.A., June.

Yang, J. and Gu, X.Q. (2013), "Shear stiffness of granular material at small strains: Does it depend on grain size?", *Geotechnique*, **63**(2), 165-179. http://doi.org/10.1680/geot.11.P.083.

Yang, J. and Liu, X. (2016), "Shear wave velocity and stiffness of sand: The role of non-plastic fines", *Geotechnique*, **66**(6), 500-514. http://doi.org/10.1680/jgeot.15.P.205.

Yang, J., Liu, X., Rahman, M.M., Lo, R., Goudarzy, M. and Schanz, T. (2018), "Shear wave velocity and stiffness of sand: The role of non-plastic fines", *Geotechnique*, **68**(10), 931-934. http://doi.org/ 10.1680/jgeot.15.P.205.

Yang, Z.X., Yang, J. and Wang, L.Z. (2013), "Micro-scale modeling of anisotropy effects on undrained behavior of granular soils", *Granul. Matter*, **15**(5), 557-572. http://doi.org/10.1007/s10035-013-0429-5.

Yu, H., Zeng, X., Li, B. and Ming, H. (2013), "Effect of Fabric Anisotropy on Liquefaction of Sand", *J. Geotech. Geoenviron. Eng.*, **139**(5), 765-774. http://doi.org/10.1061/(ASCE)GT.1943-5606.0000807.

Zhao, S., Zhang, N., Zhou, X. and Zhang, L. (2017), "Particle shape effects on fabric of granular random packing", *Powder Technol.*, **310**, 175-186. http://doi.org/10.1016/j.powtec.2016.12.094.

Zhou, Z.Y., Zou, R.P. and Pinson, D. (2011), "Dynamic simulation of the packing of ellipsoidal particles", *Industr. Eng. Chem. Res.*, **50**(16), 9787-9798. http://doi.org/10.1021/ie200862n.

IC